Author(s): Pulkkinen, Tuija I. & Partamies, N & Kissinger, J. & McPherron, R. L. & Glassmeier, K.-H. & Carlson, C.

Title: Plasma sheet magnetic fields and flows during steady magnetospheric convection events

Year: 2013

Version: Final published version

Please cite the original version:

Pulkkinen, Tuija I. & Partamies, N & Kissinger, J. & McPherron, R. L. & Glassmeier, K.-H. & Carlson, C. 2013. Plasma sheet magnetic fields and flows during steady magnetospheric convection events. Journal of Geophysical Research: Space physics, Vol. 118, nro 10. P. 6136-6144. ISSN 2169-9402 (electronic). DOI: 10.1002/jgra.50574.

Plasma sheet magnetic fields and flows during steady magnetospheric convection events

T. I. Pulkkinen,[1] N. Partamies,[2] J. Kissinger,[3] R. L. McPherron,[4]
K.-H. Glassmeier,[5] and C. Carlson[6]

Received 25 June 2013; revised 11 September 2013; accepted 14 September 2013; published 3 October 2013.

[1] Inner magnetosphere magnetic field and plasma flow data are examined during 228 steady magnetospheric convection events. We find that the B_Z component of the magnetic field around geostationary orbit is weaker than during average conditions and the plasma flow speeds are higher than average in the dusk sector just beyond geostationary orbit. The steady magnetospheric convection periods include more enhanced earthward and tailward flow intervals than during average conditions. The steady convection period magnetic field is not steady: The near-geostationary nightside field grows increasingly taillike throughout the steady convection period. In the midtail, earthward flows are enhanced in a wide region around the midnight sector, which leads to enhanced magnetic flux transport toward the Earth during the steady convection periods. Compared to well-known characteristics during magnetospheric substorms, the inner tail evolution resembles that during the substorm growth phase, while the midtail flow characteristics during steady convection periods are similar to those found during substorm recovery phases.

Citation: Pulkkinen, T. I., N. Partamies, J. Kissinger, R. L. McPherron, K.-H. Glassmeier, and C. Carlson (2013), Plasma sheet magnetic fields and flows during steady magnetospheric convection events, *J. Geophys. Res. Space Physics*, *118*, 6136–6144, doi:10.1002/jgra.50574.

1. Introduction

[2] Following the discovery of the interplanetary magnetic field by Pioneer V spacecraft, *Dungey* [1961] postulated that the interaction of that field with the geomagnetic dipole would set up a large-scale plasma circulation pattern in which plasma would flow from the solar wind into the magnetosphere and back to the solar wind powered by magnetic reconnection active both in the dayside and nightside boundaries of the Earth's magnetic cavity, the magnetosphere. Soon after, it was observationally shown [*Akasofu*, 1964] and later theoretically demonstrated [*Klimas et al.*, 1994] that this circulation was not in steady state, but occurred in bursts recurring at quasi-regular intervals.

[3] *Caan and McPherron* [1973] reported on an event when enhanced energy input did not lead to repetitive loading—unloading cycle, but rather "a state of continual geomagnetic activity with no clearly defined substorm phases." *Pytte et al.* [1978] examined these events in more detail and concluded that "substorm expansions are not the main cause of this activity and that convection bays are phenomenologically different from polar magnetic substorms." *Yahnin et al.* [1994] coined the term "steady magnetospheric convection" (SMC) to the phenomenon and showed its association with small-scale auroral activations within a wide "double oval" configuration. *Sergeev et al.* [1996] summarizes modeling results revealing that the inner plasma sheet is thin and has a stretched magnetic field, while the midtail plasma sheet is thick with an enhanced B_Z.

[4] Statistical surveys of steady convection intervals have shown that they typically occur during moderate, steady solar wind driving (typical values of the interplanetary electric field in the range of ∼1 mV/m) [e.g., *O'Brien et al.*, 2002] and a relatively constant polar cap size [*DeJong and Clauer*, 2005], which led *DeJong et al.* [2008] to propose yet another name "balanced reconnection interval" to the phenomenon. The balanced dayside and nightside reconnection during such events was further corroborated by modeling the Dungey cycle in the ionosphere using the "expanding/contracting polar cap paradigm" [*Milan et al.*, 2007]. *Partamies et al.* [2009a] compared substorms, sawtooth events (quasiperiodic large substorms that have a wide local time extent) [see, e.g., *Pulkkinen et al.*, 2006], and steady convection events as well as their solar wind drivers, and concluded that the steady convection events occur during solar wind electric fields that are weaker than those observed during sawtooth events. Especially noteworthy in their results was the lower value of the solar wind speed

[1]School of Electrical Engineering, Aalto University, Helsinki, Finland.
[2]Finnish Meteorological Institute, Helsinki, Finland.
[3]Goddard Space Flight Center, Greenbelt, Maryland.
[4]Department of Earth and Space Sciences, University of California, Los Angeles, California, USA.
[5]Institut für Geophysik und Extraterrestrische Physik, Technische Universität Braunschweig, Braunschweig, Germany.
[6]Space Sciences Laboratory, University of California, Berkeley, California, USA.

Corresponding author: T. I. Pulkkinen, Aalto University School of Electrical Engineering, PO Box 11000, 00076 Aalto, Finland. (tuija.pulkkinen@aalto.fi)

2169-9380/13/10.1002/jgra.50574

during steady convection periods than during sawtooth events. This result is indirectly supported by analysis in *Pulkkinen et al.* [2007], who concluded that for the same value of the solar wind electric field, higher solar wind speed will lead to higher level of magnetospheric activity.

[5] The steady convection event characteristics and occurrence frequency over a solar cycle was recently examined by *Kissinger et al.* [2010, 2011, 2012] using a large statistical database. Even though coronal mass ejections (CME) often include intervals of steady solar wind parameters, they found no correlation between CME and steady convection event occurrence. Instead, a clear association was made with the stream interfaces that often involve weaker driving, even if not quite as stable magnetic field structure. Furthermore, *Kissinger et al.* [2012] conclude that during steady convection events, the midtail fast flows are more frequent, the plasma is of lower density and higher temperature than during quiet conditions.

[6] Here we return to the question of magnetotail characteristics during steady convection intervals using the unique opportunity provided by the five-spacecraft Time History of Events and Macroscale Interactions during Substorms (THEMIS) mission [*Angelopoulos*, 2008] that provides multipoint observations during extended periods in the inner magnetosphere. We focus on the inner magnetosphere average flows as well as the magnetic field structure and its evolution during these events. Section 2 describes the data set, sections 3 and 4 discuss the average conditions during steady convection events, while section 5 examines the temporal evolution of the steady convection events. Section 6 concludes with discussion.

2. Data

[7] In this analysis, the steady convection events are selected from a list compiled by *Kissinger et al.* [2010] consisting of about 3000 steady convection events observed during 1997–2009. The event selection was based on auroral electrojet indices. It was required that both the upper AU index and lower AL index show ongoing activity with $AU > 50$ nT and $AL < -75$ nT and that no substorm signatures or other rapid variations were recorded in the AL index with $-7.4 < dAL/dt < 10$ nT/min using a 15 min sliding derivative operator. Furthermore, the events were required to last longer than 90 min such that at least 90% of points in a given interval satisfy all the above criteria [*Kissinger et al.*, 2010].

[8] From this data set, we utilize the period from late 2007 to the end of 2009 during which observations from the THEMIS constellation mission are available, amounting to 228 SMC events. The THEMIS mission comprises five identical satellites on orbits enabling recurrent probe alignments parallel to the Sun-Earth line (within 2 R_E in the Y direction from each other). The spacecraft can thus monitor tail phenomena simultaneously at ~10 R_E and at ~20–30 R_E downtail while mapping magnetically over a network of ground-based observatories hosting magnetic and optical instruments [*Angelopoulos*, 2008]. Figure 1 illustrates the power of the five-spacecraft mission: The event shown (discussed in more detail below) includes measurements from all five spacecraft with the innermost probe at about $X = -8$ R_E, two craft around $X = -10$ R_E, one just earthward of -20 R_E,

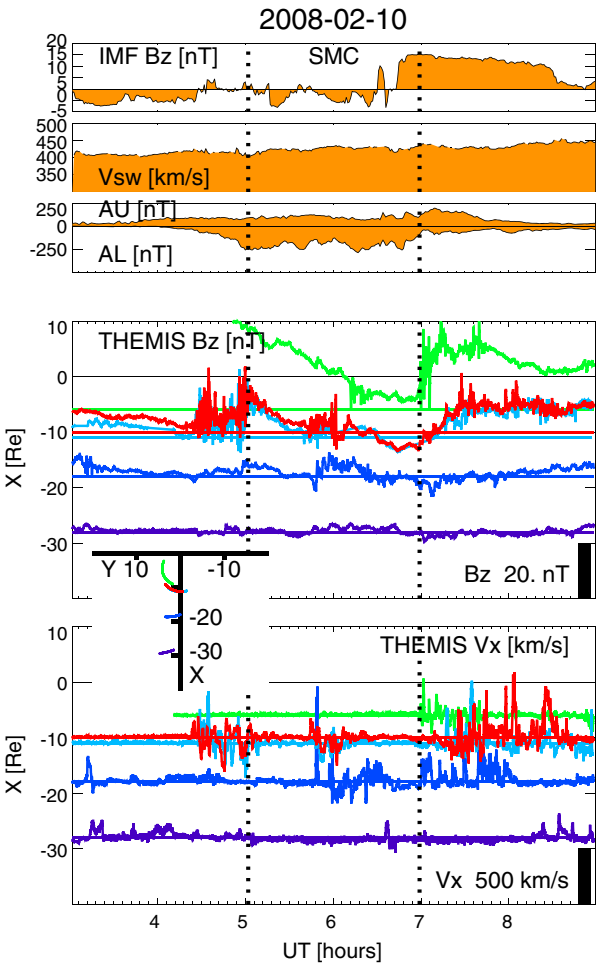

Figure 1. Sample steady convection event on 10 February 2008. (top) Interplanetary magnetic field B_Z in nT, solar wind speed in km/s, and auroral electrojet indices AU and AL in nT. (middle) Magnetic field B_Z component from all five THEMIS spacecraft are shown with the scale in nT indicated at the bottom right corner of the panel. Reference levels shown by horizontal lines indicate the satellite X distance during the middle of the interval in the axis shown on the left. (bottom) Plasma velocity V_X component in km/s from all THEMIS spacecraft. Reference levels are chosen as above. The insert shows the spacecraft orbit segments in the GSM XY plane during the event with the same color coding as in the data plots.

and the most outward satellite at $X = -30$ R_E, all relatively close to local midnight sector (the insert shows orbit segments during the event in an equatorial plane projection).

[9] Figure 2 (top row) shows the distribution of orbit segments from all spacecraft projected in the geocentric solar magnetospheric (GSM) coordinate XY and XZ planes during the steady convection events. As the spacecraft apogee are in the nightside only a few months each year, only a subset of the events has measurements from the region tailward of 20 R_E, which limits the statistical analysis in that region. Most of the data were recorded close to the equatorial plane within the plasma sheet. However, no attempt was made to remove lobe observations from the data set, and thus, the data set may contain a small number of data points outside

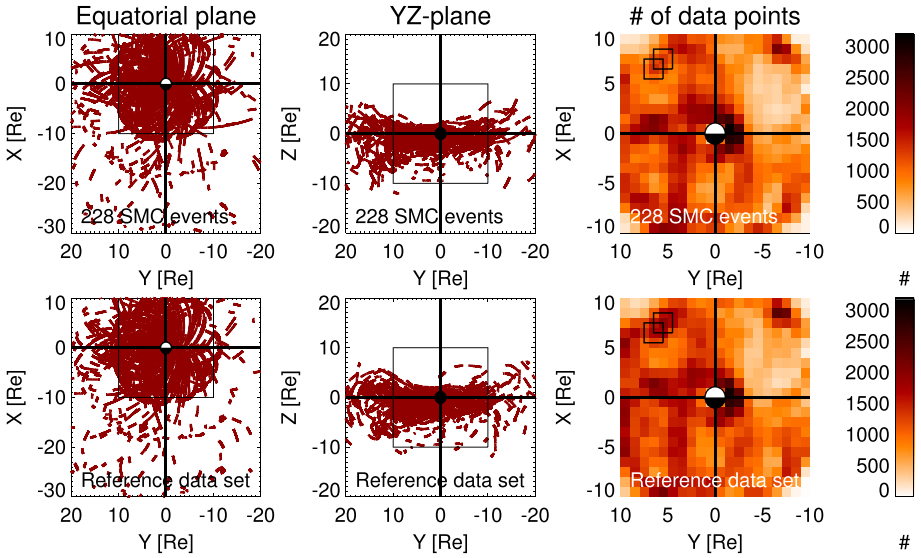

Figure 2. THEMIS spacecraft orbit segments projected in (left column) GSM *XY* and (middle column) *YZ* planes during (top row) 228 steady convection events (SMC) and (bottom row) 228 reference events. (right column) Number of 1 min averaged data points in 2 R_E by 2 R_E overlapping bins during 228 SMC events and 228 reference events within the inner magnetosphere $-10 < X < 10$ R_E and $-10 < Y < 10$ R_E. The square in the left and middle columns outlines the volume within which the statistical analysis was conducted.

the plasma sheet. The black 10 by 10 R_E rectangles in the left and middle columns show the volume within which observations were considered in the statistics shown in the right column.

[10] In order to compare the results obtained during the SMC events with those during other conditions, we created a reference data set consisting of random solar wind and magnetospheric conditions. As the results may depend on UT, season, and/or solar cycle phase, we compiled the data set by taking the durations of the SMC events, but 3 days earlier. This way the statistical coverage, seasonal, and UT dependence will be similar between the SMC data set and the reference data set. The spatial coverage of the reference data set is shown in Figure 2 (bottom row).

[11] Figure 2 (right column) shows the inner magnetosphere data coverage color coded, using 1 min averaged measurements in each bin. In order to increase counting statistics, we compute averages for each 1 R_E by 1 R_E bins but increase the bin size by taking observations from bin center to ± 1 R_E both in X and Y directions, resulting in averaging bin size of 2×2 R_E^2. Two sample averaging bins are over plotted in black in the top left corner of the coverage plots. In addition to increasing statistics, this also leads to smoothing of the data.

[12] The magnetotail plasma and electromagnetic field properties are analyzed using spin-averaged measurements from all five THEMIS spacecraft. We use spin-averaged magnetic field measurements from the fluxgate magnetometer (FGM) [*Auster et al.*, 2008] and the plasma moments (density and velocity) from the electrostatic analyzer (ESA) [*McFadden et al.*, 2008]. These data were averaged to 1 min values and combined with spacecraft position information to allow comparison of both temporal and spatial effects.

[13] The solar wind driver properties and geomagnetic activity in the ionosphere were analyzed using the multisource OMNI data set compiled at National Space Science Data Center (NSSDC) (http://spdf.gsfc.nasa.gov/). The data set provides 1 min values of the solar wind plasma density and velocity, the interplanetary magnetic field, and the auroral electrojet indices. The upstream observations come from a variety of spacecraft; time delays from the satellite position to the subsolar magnetopause are accounted for by appropriate propagation of the observations (see *King* [2005] for data processing and propagation methods).

[14] Figure 1 (top) shows time series of the IMF B_Z, solar wind speed, *AU* and *AL* indices during a sample event on 10 February, 03–09 UT. The following blocks show the magnetotail magnetic field B_Z component and sunward flow velocity V_X component (in GSM coordinates). Data from the five THEMIS spacecraft are plotted such that each spacecraft has its reference zero line at the X value where the spacecraft was at the middle of the SMC event (06 UT). As the insert illustrating the orbit segments in the *XY* plane show, all observations come from near the midnight sector. The B_Z component at all five locations decreased quite steadily toward the end of the event. The V_X in the inner magnetosphere was very small, but flow burst was observed both before the event around 10 R_E and during the event at 10–20 R_E. The largest flows were observed after the event, ranging from the inner parts of the magnetosphere out to $X = -20$ R_E.

3. Inner Magnetosphere Magnetic Field

[15] The plasma motion in the inner magnetosphere is mostly governed by the magnitude of the magnetic field component perpendicular to the current sheet, which we here approximate by the GSM B_Z component. Figure 3 shows the inner magnetosphere magnetic field B_Z component with the internal field subtracted using the International Geomagnetic

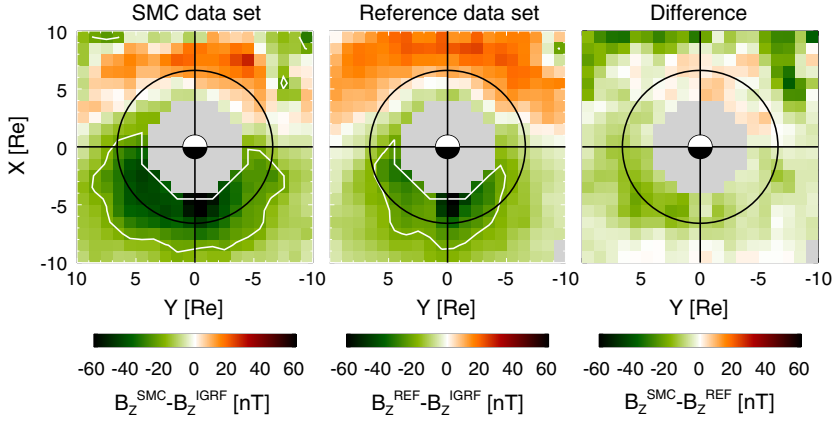

Figure 3. Inner magnetosphere magnetic field B_Z component observations with IGRF field subtracted during (left) steady convection (SMC) periods and (middle) reference periods. (right) Difference $\Delta B_Z = B_Z^{\mathrm{SMC}} - B_Z^{\mathrm{REF}}$ indicating the areas where the field during steady convection periods differs from the average over all solar wind conditions. The color coding shows positive colors in red and negative colors in green; the analysis is limited to outside 4 R_E.

Reference Field (IGRF) model. Figure 3 (left) shows B_Z during the steady convection events, while Figure 3 (middle) shows the same during the reference events. Positive values (shown with red colors) indicate that the field is larger than the internal (dipole) component. In the dayside, the field values above the dipole strength are a sign of dayside compression caused by the solar wind dynamic pressure. Note that the compression is weaker during the steady convection events, which indicates a stronger ring current in the inner magnetosphere. In the nightside, the field values are strongly negative during the steady convection events, indicating an enhanced cross-tail and ring current especially in the evening sector magnetotail.

[16] Figure 3 (right) shows the difference between the steady convection and reference data sets. Negative values indicate that the field during steady convection periods is below that during the reference times, and this is true for most of the inner magnetosphere. The darker green colors in the evening sector tail are a measure of the enhancement of the cross-tail and ring currents, while the green and red colors in the dayside also reflect differences in the average size of the magnetosphere during the steady convection and reference events.

[17] Figure 4 examines the field evolution during steady convection periods in more detail. The five frames show 15 min average periods before, during the early phase, at the middle of the event, at the end of the event, and 15 min after the steady convection event. While the "steady convection events" are indeed quite steady, there are clear and repeatable changes in the field configuration: The steady convection events often begin with a substorm, and thus, the cross-tail current is quite weak and the magnetic field is not very stretched at the beginning of the event [*DeJong et al.*, 2009]. The current intensifies during the event, but as the steady convection events often end with another substorm, the field after the event is again more dipolar [*McPherron et al.*, 2005]. The key result is that the field configuration undergoes a systematic evolution from a more dipolar toward a more stretched configuration during steady convection events. In this sense, the field evolution resembles

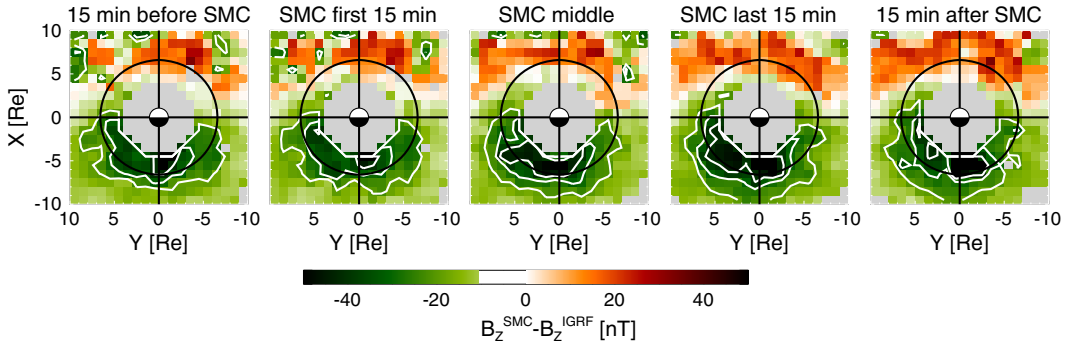

Figure 4. Temporal evolution of B_Z during the steady convection events. IGRF field has been subtracted from the measured values. The five frames show 15 min period prior to the steady convection event start, first 15 min of the event, 15 min at the middle of the event, last 15 min, and 15–30 min after the end of the steady convection event. The color coding shows positive colors in red and negative colors in green; the analysis is limited to outside 4 R_E.

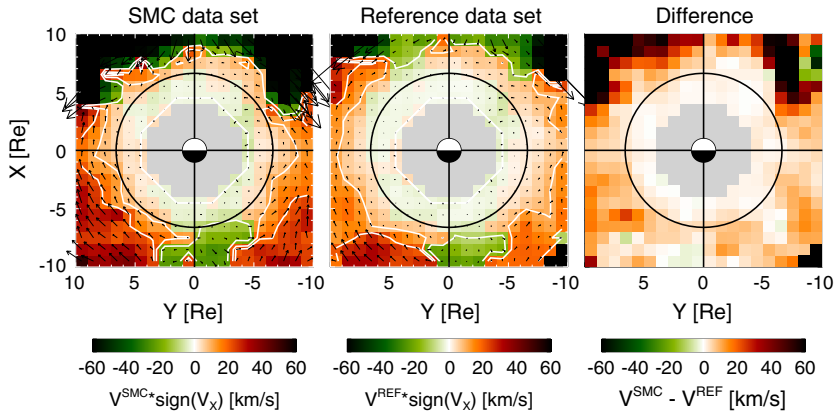

Figure 5. Plasma flow speed in the GSM XY plane ($V = \sqrt{V_X^2 + V_Y^2}$). The flow speed is multiplied by the sign of the flow V_X component in order to differentiate predominantly sunward and tailward flows. The arrows indicate the average flow direction and magnitude. (left) Steady convection events, (middle) reference data set, and (right) difference between the flow speeds ($\Delta V = V^{\mathrm{SMC}} - V^{\mathrm{REF}}$ without the sign(V_X) multiplication).

that of an extended substorm growth phase. As the steady convection events can last anywhere from 90 min (artificially set definition of minimum duration) to 5–6 h, the temporal changes are difficult to identify as they progress slowly and are masked by the spacecraft motion across the magnetosphere.

4. Plasma Sheet Flow

[18] In order to deduce the plasma transport in the magnetotail, we examine the average values of the plasma sheet flow speed (V). Figure 5 shows in color coding the average flows in the plasma sheet during steady convection periods (left) and computed from the reference data set (middle).

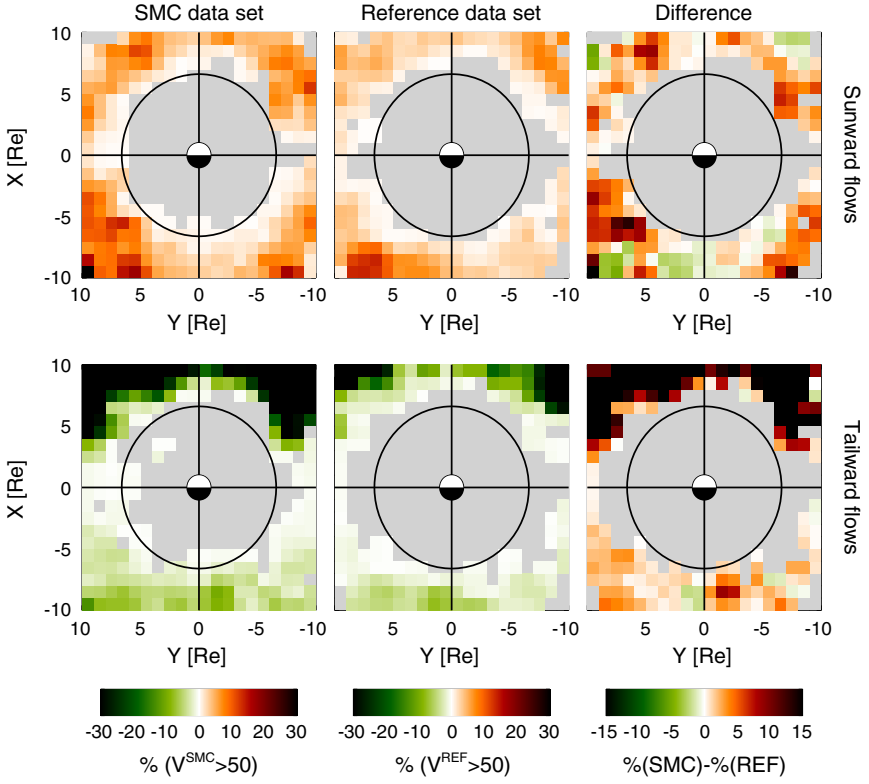

Figure 6. Percentage of observations during which 1 min averaged flow speed exceeds 50 km/s during (left column) steady convection periods and (middle column) reference periods. The flow data set is divided into predominantly (top row) sunward ($V_X > 0$, red colors) and (bottom row) tailward ($V_X < 0$, green colors). (right column) The differences of the two percentages with positive values in red colors and negative values in green colors.

The plasma sheet flows are computed in the GSM XY plane using the V_X and V_Y components ($V^2 = V_X^2 + V_Y^2$). In order to distinguish earthward and tailward flows in the plot, the flow speed is multiplied by the sign of the V_X component. The overplotted black arrows indicate the flow magnitude and direction in the GSM XY plane.

[19] Both the steady convection data set and the reference data set show the earthward and duskward flow in the evening sector, and a slow tailward return flow in the early morning sector tailward of geostationary orbit (outside 6.6 R_E). The flows inward and tailward are stronger during the steady convection events. For the same level of external solar wind driver electric field, the smaller B_Z in the tail will lead to higher $\mathbf{E} \times \mathbf{B}$ drift speed and hence plasma transport toward the inner magnetosphere. Note that overall, the flow speeds are quite low in this region.

[20] Figure 5 (right) shows the difference between the steady convection periods and reference events, with red colors indicating that the speed is larger during the steady convection events than during the reference events. It is evident also in this representation that the flow speeds increase during the steady convection periods in the inner parts of the magnetosphere.

[21] The flows in the magnetosphere are not steady, but for the most part occur in short bursts that have lifetimes from tens of seconds to a few minutes [*Angelopoulos et al.*, 1993]. Thus, changes in the magnetotail configuration and dynamics are not only controlled by changes in the average flow speed patterns but also by the occurrence frequency of such flow bursts. As the flows slow down quite considerably as the dipole field component increases [*Shiokawa et al.*, 1997], the flows are not "fast" in this region in the sense usually understood when analyzing observations deeper in the magnetotail (several hundred km/s). Here we have defined a "flow event" to be a 1 min average sample with averaged flow speed in excess of 50 km/s.

[22] Figure 6 shows the percentages of observations during which the 1 min averaged flow speed is larger than 50 km/s. Figure 6 (left column) shows results for the steady convection events, and Figure 6 (middle column) shows the reference data set analysis. In this case, we have separated the data set into two, with Figure 6 (top row) containing those measurements where the flow is predominantly sunward ($V_X > 0$) and Figure 6 (bottom row) containing measurements with predominantly tailward ($V_X < 0$).

[23] Comparing the steady convection and reference events, one can see that flow bursts during the reference period are virtually absent in the vicinity of the geostationary orbit. During the steady convection events, the occurrence frequency of the flow bursts in the inner parts of the magnetosphere increases, but remains relatively low. Also at larger distances in the tail, both earthward and tailward flow bursts are more common during the steady convection events than during the reference periods. The same result can be concluded from Figure 6 (right column), which illustrate the differences between the steady convection and reference data sets. Especially noteworthy is the region near midnight, where the sunward flows are less frequent during the steady convection periods (green colors in Figure 6, top row), while the tailward flows are more numerous during the steady convection events (red colors in Figure 6, bottom row).

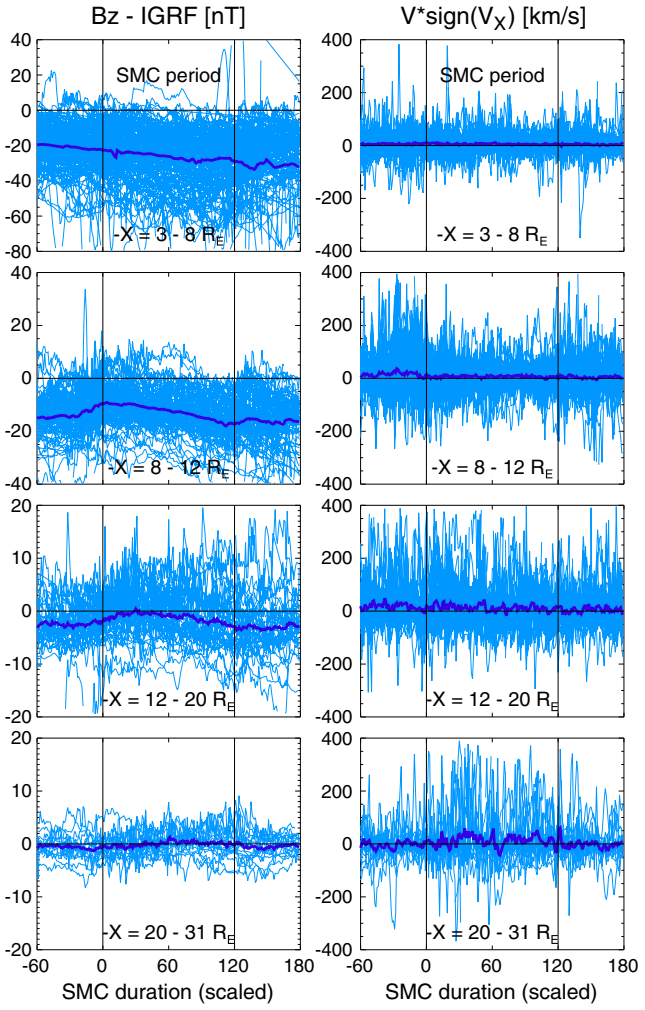

Figure 7. Superposed epoch analysis during steady convection periods of the magnetic field (left) B_Z component (IGRF field subtracted) and (right) flow V_X component at different distances from the Earth as indicated. Only observations where the spacecraft are in the central part of the tail ($|Y| < 10\ R_E$) are included in the analysis. The SMC period durations are scaled to artificial time with all events starting at $T = 0$ and ending at $T = 120$. Periods leading to and following the steady convection events are also shown. Note that the statistics in the two most tailward bins is limited.

5. Superposed Epoch Analysis of Magnetotail Evolution

[24] To further examine the temporal evolution during the events as well as the radial dependence of the changes, we divided the observations into different bins based on the spacecraft position at the middle of the event. The bins in X distance were chosen to be $-3 \ldots -8\ R_E$, $-8 \ldots -12\ R_E$, $-12 \ldots -20\ R_E$, and $-20 \ldots -31\ R_E$. Furthermore, the analysis was limited to observations at the center of the tail with $|Y| < 10\ R_E$. In order to deduce the average evolution during the event duration, each event was scaled to similar time frame with event start at $T = 0$ and event end at $T = 120$. As the average duration of the events is slightly over 2 h, for average events, the time scale would be in minutes.

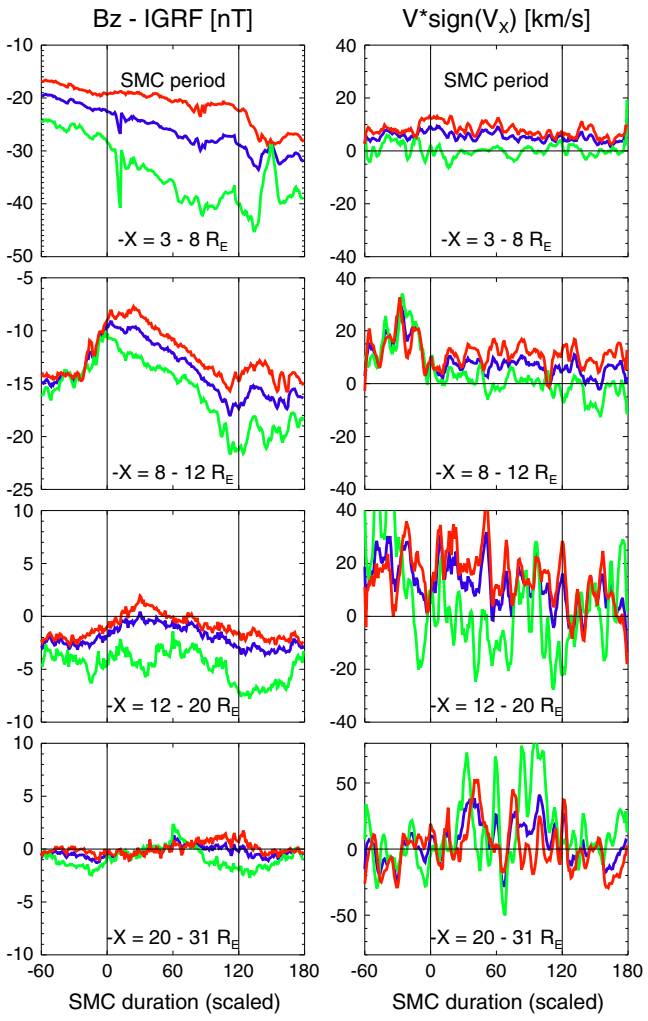

Figure 8. Superposed epoch analysis during steady convection periods of the (left) magnetic field B_Z component (IGRF field subtracted) and (right) flow speed multiplied by the sign of V_X at different distances from the Earth as indicated. Data shown in blue are the same as in Figure 7 with smoothing applied to the flow data. The green curves show superposed epoch analysis results in the Y range $|Y| < 3\ R_E$, while the red curves show superposed epoch results in the Y range $3\ R_E < |Y| < 10\ R_E$.

[25] Figure 7 shows the results of the superposed epoch analysis. Figure 7 (left) shows the magnetic field evolution with dipole field subtracted, while Figure 7 (right) shows the flow speed multiplied by the sign of V_X. The panels show the individual events (with time scaled as discussed above) in blue and the superposed epoch results in dark blue.

[26] Figure 8 shows the superposed epoch results in an expanded Y scale to better illustrate the temporal changes. The blue curves are the same as shown in Figure 7, with the exception that the flow speed data has been slightly smoothed. The red and green curves show two subsets of data: the green curves show data from the tail center $|Y| < 3\ R_E$, and the red curves show data from the flanks with $3\ R_E < |Y| < 10\ R_E$. It is clear that the midtail magnetic field is more stretched than that closer to the flanks (B_Z is smaller), while the temporal evolution is similar at all Y values (inside 10 R_E). The inner magnetosphere flow speed is smallest close to midnight, while the flank flows are typically positive. In the most distant part of the tail, the flow patterns are similar for all Y values.

[27] The inner magnetosphere field depression during the steady convection events is quite evident in the data, especially in the range 8–12 R_E in the nightside tail. In the midtail, the B_Z component enhances during the event, while in the more distant part of the tail, the magnetic field does not show consistent changes.

[28] The flow speeds do not show similarly coherent temporal evolution. Looking at the general patterns in Figure 8 (right, first and second panels), one could argue that the flows actually somewhat slow down in the inner magnetosphere, while they are activated in the most distant part of the tail.

6. Discussion and Conclusions

[29] *Kissinger et al.* [2012] in their comprehensive study of magnetotail properties during substorms and steady convection events conclude that the probability of fast flows in the midtail is higher during steady convection events than even during substorm recovery phase, when the flows maximize in the substorm cycle. Furthermore, the midtail flux transport was at high level, while no signs of localized flow channel at the tail center was evident during steady convection events. In the inner magnetosphere, *Kissinger et al.* [2012] note that the flows are deflected in duskward direction, and the earthward transport rate is smaller than during the substorm cycle.

[30] Analysis in this paper corroborate the above results in the inner magnetosphere: The magnetic field around geostationary orbit is weaker than during average conditions (the field is more stretched or taillike than average), and the plasma flow speeds are higher than average in the dusk sector just beyond geostationary orbit. The inner magnetosphere typically does not involve strong flows, but looking at 1 min intervals of flows in excess of 50 km/s, it is evident that the SMC periods include more such flow intervals directed both in the earthward and tailward directions than the reference data set. Thus, the flows in the inner magnetosphere are more bursty and more irregular than during average conditions.

[31] This study adds to the earlier studies by demonstrating the temporal evolution of the inner magnetosphere field structure during the steady convection events: The near-geostationary nightside field grows increasingly taillike throughout the evolution of the steady convection period before a dipolarization takes place at the end of the event. Similar temporal evolution could not be resolved from the flow data, rather the flows are irregular and have a variance above that during average conditions. In our data set, neither the magnetic field nor plasma flows showed significant temporal evolution in the midtail; rather the flows were enhanced throughout the event, while the magnetic field B_Z component remained relatively stagnant.

[32] In studies of phenomenologically defined objects such as steady convection events, magnetospheric substorms, sawtooth events or magnetic storms, a key question is to determine to what extent they are caused by distinct physical processes and to what extent they are independent

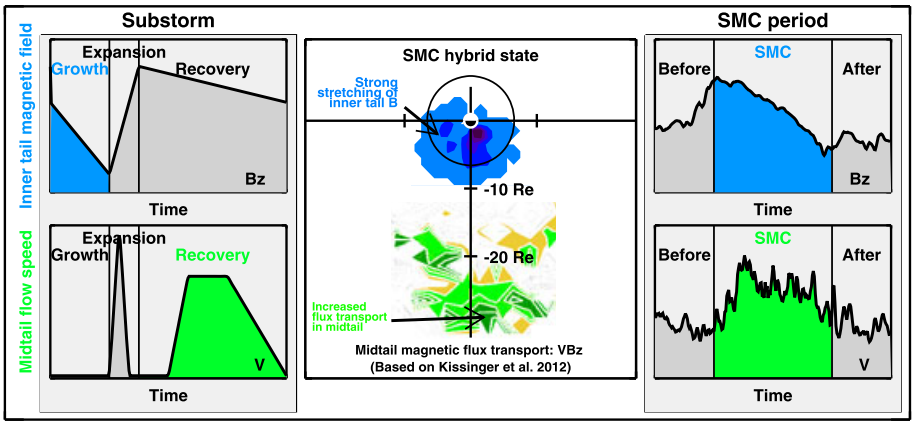

Figure 9. Schematic comparison of (left) magnetospheric substorms and (right) steady convection events. (top) Inner tail magnetic field and (bottom) midtail plasma flow speed temporal evolution during magnetospheric substorms and during steady convection events. The substorm illustration is a schematic understanding of the substorm growth, expansion, and recovery phases [see, e.g., *Baker et al.*, 1996]. Qualitatively similar temporal evolution is highlighted in blue and green colors. (middle) Illustration of the hybrid state of the magnetotail in the equatorial plane. Inner magnetic field stretching is shown based on data shown in Figure 4. Midtail magnetic flux transport is illustrated by a graph based on results by *Kissinger et al.* [2012] showing a strong enhancement of flux transport in the region tailward of about –20 R_E. Note that the inner tail evolution during SMC resembles that of the substorm growth phase, while the midtail evolution during SMC is similar to substorm recovery phase.

phenomena rather than peaks in a continuum of activity levels ranging from quiet to highly disturbed. The strong dependence of the magnetospheric response on the solar wind driver—and the high variability of that driver—create a great variance within the event categories and thus make statistical analysis as well as unique identification of physical processes challenging. Earlier studies have concluded that sawtooth events and activations within storms have basically the same building blocks as substorms, and thus, the differences in appearance are more caused by the level and variability of external driving and the level of background disturbances [*Partamies et al.*, 2009a, 2009b; *Pulkkinen et al.*, 2006, 2007].

[33] Figure 9 summarizes our current understanding of the magnetospheric configuration during steady convection events in a schematic illustration. In the inner magnetosphere, the magnetic field is not constant but grows continuously more taillike during the steady convection period. At the end of the event, the magnetic field changes back toward more dipolar shape. In the midtail, earthward flows are enhanced in a wide region around the midnight sector, which leads to enhanced magnetic flux transport toward the Earth during the steady convection periods. Compared to well-known characteristics during magnetospheric substorms, the inner tail evolution resembles that during the substorm growth phase (Figure 9, top left). The midtail flow characteristics during steady convection periods are similar to those found during substorm recovery phases, when the plasma sheet is refilled after a large-scale reconfiguration and reconnection event. Thus, one could hypothesize that the enhanced flow illustrated in Figure 9 (bottom right) is similar to that during the substorm recovery phase, and therefore also caused by a large-scale reconnection event in the midmagnetotail.

[34] For the steady convection events, open questions include what prohibits the inner tail instability to develop earlier despite energy loading from the solar wind, and what maintains the reconnection region in the midtail active over the extended steady convection period. A possible reason for the inner tail stability is that the flows do not reach the inner magnetosphere, and thus, the magnetic field does not become sufficiently stretched for an instability to develop. While many substorms are triggered by rapid northward turnings of the interplanetary magnetic field [*Hsu*, 2002], the steady convection data set did not include a statistically significant fraction of events during which the IMF would have turned northward close to the end time of the event: Visual inspection of the solar wind data showed that about 20% of the events can be interpreted to end with a "substorm onset" or *AL* enhancement, and a similar portion of events show a northward IMF turning within about 15 min of the end time. In the total statistics, the northward turnings are not more frequent at the steady convection end time than during other times (not shown). Thus, while IMF northward turnings may contribute to substorm triggering at the end of some steady convection events, northward turnings are not a major cause for the steady convection events to end.

[35] The auroral precipitation pattern during steady convection events resembles an active substorm recovery phase with a thick and bright oval and often a double oval configuration [*Yahnin et al.*, 1994] with weaker emissions between bright equatorward and poleward boundaries. The auroral evolution may include poleward boundary intensifications that often end as auroral streamers propagating equatorward [*Sergeev*, 2001]. It is clear that the poleward boundary maps to very large distances in the magnetotail. As the inner magnetosphere tail stretches, the loss cone becomes smaller and fewer particles have access to the ionosphere hence creating a band of weak or no auroral emissions. The larger loss cone and brighter precipitation at the inner edge contribute to the double oval configuration. The equatorward propagating auroral activations have been associated with midtail flows

[*Nakamura et al.*, 2001], and it is likely true here also—the midtail flow bursts typical of the steady convection intervals give rise to auroral streamers initiated close to the poleward boundary and traveling toward the equatorward boundary.

[36] With these results, we can provide a tentative answer to a thus-far unresolved question of what ends the steady convection events: If the inner tail magnetic field is continuously stretched, it is evident that at some point, an instability will set up in the inner magnetosphere. In this regard, the steady convection periods are like extended growth phases in the inner magnetosphere. Note that this conclusion is different from earlier studies, which have assumed that the magnetic configuration remains unchanged during the steady convection period. The enhanced midtail magnetic flux transport contributes to the field evolution by transporting magnetic flux into the inner magnetosphere region, while simultaneously maintaining the magnetic field B_Z component positive throughout the period, which of course prevents the growth of large-scale reconnection events in that region. Thus, while the inner magnetotail continuously evolves toward an increasingly unstable state, the midtail large earthward flux transport with predominantly northward B_Z component slows down the development toward an unstable state leading to a quasi-stationary configuration in a large portion of the magnetosphere.

[37] **Acknowledgments.** We thank the THEMIS team for making the data available in a readily accessible format. We thank the NSSDC for providing the solar wind and interplanetary field measurements and their work for propagating the disturbance fronts to the Earth orbit. T.P. thanks Minna Palmroth for useful discussions. The work by K.H.G. was financially supported by the German Ministerium für Wirtschaft und Technologie and the Deutsches Zentrum für Luft- und Raumfahrt under grants 50OC1102 and 50OC1001.

[38] Masaki Fujimoto thanks Anita Kullen and an anonymous reviewer for their assistance in evaluating this paper.

References

Akasofu, S.-I. (1964), The development of the auroral substorm, *Planet. Space Sci.*, *12*, 273–282.

Angelopoulos, V. (2008), The THEMIS mission, *Space Sci. Rev.*, *141*(1-4), 5–34.

Angelopoulos, V., C. F. Kennel, F. V. Coroniti, R. Pellat, M. G. Kivelson, R. J. Walker, C. T. Russell, H. E. Spence, W. Baumjohann, and W. C. Feldman (1993), Characteristics of ion flow in the quiet state of the inner plasma sheet, *Geophys. Res. Lett.*, *20*(16), 1711–1744.

Auster, H. U., et al. (2008), The THEMIS fluxgate magnetometer, *Space Sci. Rev.*, *141*(1-4), 235–264.

Baker, D. N., T. I. Pulkkinen, V. Angelopoulos, W. Baumjohann, and R. L. McPherron (1996), The neutral line model of substorms: Past results and present view, *J. Geophys. Res.*, *101*, 12,975–13,010.

Caan, M. N., and R. F. McPherron (1973), Solar wind and substorm-related changes in the lobes of the geomagnetic tail, *J. Geophys. Res.*, *78*, 8087–8096.

DeJong, A. D., A. J. Ridley, X. Cai, and C. R. Clauer (2009), A statistical study of BRIs (SMCs), isolated substorms, and individual sawtooth injections, *J. Geophys. Res.*, *114*, A08215, doi:10.1029/2008JA013870.

DeJong, A. D., A. J. Ridley, and C. R. Clauer (2008), Balanced reconnection intervals: Four case studies, *Ann. Geophys.*, *26*, 3897–3912.

DeJong, A. D., and C. R. Clauer (2005), Polar UVI images to study steady magnetospheric convection events: Initial results, *Geophys. Res. Lett.*, *32*, L24101, doi:10.1029/2005GL024498.

Dungey, J. (1961), Interplanetary magnetic field and the auroral zones, *Phys. Rev. Lett.*, *6*(2), 47–48.

Hsu, T.-S. (2002), An evaluation of the statistical significance of the association between northward turnings of the interplanetary magnetic field and substorm expansion onsets, *J. Geophys. Res.*, *107*(A11), 1398, doi:10.1029/2000JA000125.

King, J. H. (2005), Solar wind spatial scales in and comparisons of hourly Wind and ACE plasma and magnetic field data, *J. Geophys. Res.*, *110*, A02104, doi:10.1029/2004JA010649.

Kissinger, J., R. L. McPherron, V. Angelopoulos, T. S. Hsu, and J. P. McFadden (2010), An investigation of the association between steady magnetospheric convection and CIR stream interfaces, *Geophys. Res. Lett.*, *37*, L04105, doi:10.1029/2009GL041541.

Kissinger, J., R. L. McPherron, T. S. Hsu, and V. Angelopoulos (2011), Steady magnetospheric convection and stream interfaces: Relationship over a solar cycle, *J. Geophys. Res.*, *116*, A00I19, doi:10.1029/2010JA015763.

Kissinger, J., R. L. McPherron, T. S. Hsu, and V. Angelopoulos (2012), Diversion of plasma due to high pressure in the inner magnetosphere during steady magnetospheric convection, *J. Geophys. Res.*, *117*, A05206, doi:10.1029/2012JA017579.

Klimas, A. J., D. N. Baker, D. Vassiliadis, and D. A. Roberts (1994), Substorm recurrence during steady and variable solar wind driving: Evidence for a normal mode in the unloading dynamics of the magnetosphere, *J. Geophys. Res.*, *99*(1), 14,855–14,861.

McFadden, J. P., C. W. Carlson, D. Larson, M. Ludlam, R. Abiad, B. Elliott, P. Turin, M. Marckwordt, and V. Angelopoulos (2008), The THEMIS ESA plasma instrument and in-flight calibration, *Space Sci. Rev.*, *141*(1-4), 277–302.

McPherron, R. L., T. P. O'Brien, and S. Thompson (2005), Solar wind drivers for steady magnetospheric convection, in *Multiscale Coupling of the Sun-Earth Processes*, edited by A. T. Y. Lui, Y. Kamide, and G. Consolini, Elsevier, Amsterdam, 113–124.

Milan, S. E., G. Provan, and B. Hubert (2007), Magnetic flux transport in the Dungey cycle: A survey of dayside and nightside reconnection rates, *J. Geophys. Res.*, *112*, A01209, doi:10.1029/2006JA011642.

Nakamura, R., W. Baumjohann, R. Schödel, M. Brittnacher, V. A. Sergeev, M. Kubyshkina, T. Mukai, and K. Liou (2001), Earthward flow bursts, auroral streamers, and small expansions, *J. Geophys. Res.*, *106*(A6), 10,791–10,802, doi:10.1029/2000JA000306.

O'Brien, T. P., S. M. Thompson, and R. L. McPherron (2002), Steady magnetospheric convection: Statistical signatures in the solar wind and AE, *Geophys. Res. Lett.*, *29*(7), 1130, doi:10.1029/2001GL014641.

Partamies, N., T. I. Pulkkinen, R. L. McPherron, K. McWilliams, C. R. Bryant, E. Tanskanen, H. J. Singer, G. D. Reeves, and M. F. Thomsen (2009a), Different magnetospheric modes: Solar wind driving and coupling efficiency, *Ann. Geophys.*, *27*, 4281–4291.

Partamies, N., T. I. Pulkkinen, R. L. McPherron, K. McWilliams, C. R. Bryant, E. Tanskanen, H. J. Singer, G. D. Reeves, and M. F. Thomsen (2009b), Statistical survey on sawtooth events, SMCs and isolated substorms, *Adv. Space Res.*, *44*(3), 376–384.

Pulkkinen, T. I., N. Y. Ganushkina, E. I. Tanskanen, M. Kubyshkina, G. D. Reeves, M. F. Thomsen, C. T. Russell, H. J. Singer, J. A. Slavin, and J. Gjerloev (2006), Magnetospheric current systems during storm-time sawtooth events, *J. Geophys. Res.*, *111*, A11S17, doi:10.1029/2006JA011627.

Pulkkinen, T. I., C. C. Goodrich, and J. G. Lyon (2007), Solar wind electric field driving of magnetospheric activity: Is it velocity or magnetic field?, *Geophys. Res. Lett.*, *34*, L21101, doi:10.1029/2007GL031011.

Pulkkinen, T. I., N. Partamies, R. L. McPherron, M. Henderson, G. D. Reeves, M. F. Thomsen, and H. J. Singer (2007), Comparative statistical analysis of storm time activations and sawtooth events, *J. Geophys. Res.*, *112*, A01205, doi:10.1029/2006JA012024.

Pytte, T., R. L. McPherron, and E. W. Hones Jr. (1978), Multiple-satellite studies of magnetospheric substorms: Distinction between polar magnetic substorms and convection-driven negative bays, *J. Geophys. Res.*, *83*, 663–679.

Sergeev, V. A. (2001), Substorm and convection bay compared: Auroral and magnetotail dynamics during convection bay, *J. Geophys. Res.*, *106*, 18,843–18,856.

Sergeev, V. A., R. J. Pellinen, and T. I. Pulkkinen (1996), Steady magnetospheric convection: A review of recent results, *Space Sci. Rev.*, *75*(3-4), 551–604.

Shiokawa, K., W. Baumjohann, and G. Haerendel (1997), Braking of high-speed flows in the near-Earth tail, *Geophys. Res. Lett.*, *24*(1), 1197–1201.

Yahnin, A. G., et al. (1994), Features of steady magnetospheric convection, *J. Geophys. Res.*, *99*, 4039–4051.